Exact Stoichiometry of CexZr6–x Cornerstones in Mixed-Metal UiO-66 Metal–Organic Frameworks Revealed by Extended X-ray Absorption Fine Structure Spectroscopy

Supporting information

Exact stoichiometry of Ce_xZr_{6-x} cornerstones in mixed-metal UiO-66 MOFs revealed by EXAFS spectroscopy

Kirill A. Lomachenko*[,1], Jannick Jacobsen[2], Aram L. Bugaev[3], Cesare Atzori[4], Francesca Bonino[4], Silvia Bordiga[4], Norbert Stock[2] and Carlo Lamberti*[,3,5]

[1]European Synchrotron Radiation Facility, 71 Avenue des Martyrs, CS 40220, 38043 Grenoble Cedex 9, France

[2]Institut für Anorganische Chemie, Christian-Albrechts-Universität, Max-Eyth-Straße 2, D 24118 Kiel, Germany

[3]Smart Materials Research Institute, Southern Federal University, Sladkova 178/24, 344090 Rostov-on-Don, Russia

[4]Department of Chemistry, NIS interdepartmental Center and INSTM Reference Center, University of Turin, Via Quarello 15, 10135 Turin, Italy

[5]Department of Physics, INSTM Reference Center and CrisDi Interdepartmental Centre for Crystallography, University of Turin, Via P. Giuria 1, 10125 Turin Italy

1. Synthesis

Cerium (IV) ammonium nitrate (98 %, $(NH_4)_2Ce(NO_3)_6$, Alfa Aesar), 1,4- benzenedicarboxyic acid (98 %, H_2BDC, Sigma Aldrich), zirconyl nitrate monohydrate ($ZrO(NO_3)_2 \cdot H_2O$, ABCR), zirconium(IV) chloride (99 %, $ZrCl_4$, Sigma Aldrich), N,N-dimethylformamide (99 %, DMF, Grüssing GmbH) and formic acid (100 %, HCOOH, BASF) were used as obtained.

The synthesis of the mixed-metal Ce/Zr-UiO-66 compounds was previously reported by Lammert et al.[1-2] and this procedure was also used in the current study. The Ce/Zr-UiO-66 compounds were synthesized using Pyrex glass reaction tubes (maximum volume 14 mL). The linker 1,4-benzenedicarboxylic acid (H_2BDC, 127.6 mg) was dissolved in N,N-dimethylformamide (DMF, 3.6 mL) and transferred into the glass reactor. Subsequently the formic acid (HCOOH, 100 %, 1.03 mL) and finally the aqueous solutions of $(NH_4)_2Ce(NO_3)_6$ (0.533 mol/L) and $ZrO(NO_3)_2 \cdot H_2O$ (0.533 mol/L) were added in the desired stoichiometry (Table S1). The total volume of the two metal salt solutions was always 1.2 mL.

Table S1 Parameters for the synthesis of the pure Ce-UiO-66 and mixed-metal Ce/Zr-UiO-66 compounds.

Sample	Ratio				Ce	Zr	H_2BDC	DMF	HCOOH
	Ce	Zr	H_2BDC	HCOOH	[μL]	[μL]	[mg]	[mL]	[μL]
Ce10	0.6	5.4	7.2	256	120	1080	127.6	3.6	1.03
Ce22	2.0	4.0	7.2	256	400	800	127.6	3.6	1.03
Ce45	4.0	2.0	7.2	256	800	400	127.6	3.6	1.03
Ce84	5.5	0.5	7.2	256	1100	100	127.6	3.6	1.03
Ce-UiO-66	6.0	0.0	7.2	256	1200	0	127.6	3.6	1.03

The glass reactors were heated under stirring for 15 min at 100 °C using an aluminium heating block. After the synthesis the glass reactor was cooled down to room temperature and the precipitate was isolated by centrifugation. The mother liquor was decanted off and the MOF were re-dispersed and centrifuged two times in DMF (2 mL) and three times in acetone (2 mL). Finally, the MOF was dried in air at 70 °C.

Zr-UiO-66 was synthesized following the procedure reported by Cavka et al.[3] Zirconium(IV) chloride (530 mg) and 1,4-benzenedicarboxylic acid (H_2BDC, 340 mg) were dissolved in N,N-dimethylformamide (DMF, 20 mL). This mixture was sealed in a steel autoclave and placed in an oven at 120 °C for 24 hours. After the synthesis the solvothermal reactor was cooled down to room temperature and the precipitate was centrifuged. The mother liquor was decanted off and the product was re-dispersed and centrifuged two times in DMF (5 mL) and three times in acetone (5 mL). Finally, the MOF was dried in air at 70 °C.

2. EDX spectroscopy

Ce/Zr ratio of the samples indicated in the samples' designations was determined by the energy-dispersive X-ray (EDX) spectroscopy. The data were recorded on a Philips XL30 FEG microscope for the samples in powder form, collecting EDX spectra in three different points to check the sample homogeneity. Obtained data are summarized in the Table S2.

Table S2 Ce content in the bimetallic CeZr-UiO-66 MOFs determined by EDX spectroscopy measured in three different points

Sample	Ce content, at%				Standard deviation, at %
	(1)	(2)	(3)	**Mean**	
Ce10	10.17	9.68	9.97	**9.94**	0.2
Ce22	21.53	21.93	22.51	**21.99**	0.40
Ce45	44.52	45.65	45.13	**45.10**	0.46
Ce84	83.65	84.22	83.65	**83.84**	0.27

3. PXRD

Powder X-ray diffraction (PXRD) measurements of the pure Ce-, pure Zr- and mixed-metal $Zr_{3.54}Ce_{2.46}$-UiO-66 MOFs desolvated at 180 °C in vacuum were conducted at the high-resolution powder diffraction beamline of the European Synchrotron Radiation Facility (ID22).

For the refinements several ranges measured for the respective sample were summed up to one pattern (10 ranges for Ce and Zr and 9 ranges for the Ce/Zr mixed-metal MOF). The used wavelength was 0.31783 Å. The peak shape function was fitted with a Pseudo Voigt profile and the beamline set-up was modelled using the simple axial model. For the Rietveld refinements, performed up to $2\theta_{max} = 32°$ ($d_{min} = 0.577$ Å) using TOPAS software,[4] the respective published crystal structures of Zr- or Ce-UiO-66 were employed as starting point. In all refinements the cluster occupancy was set to 1 and the occupancy of the linker molecules was freely refined. For the mixed-metal MOF the metal ions were refined independently of each other and their summed occupancy was fixed to one. In all MOFs traces of electron density were observed by Fourier synthesis inside the pores and attributed to residual solvent molecules represented by partially occupied oxygen atoms which were freely refined. Distance restrains were applied for the C-O and C-C bonds and the O-O distance of the carboxylate group. Collected data and results of refinement are shown in Figure S1, Figure S2, Figure S3 and Table S3. In all samples, all observed Bragg peaks belong to the UiO-66 phase and no crystalline impurity could be detected.

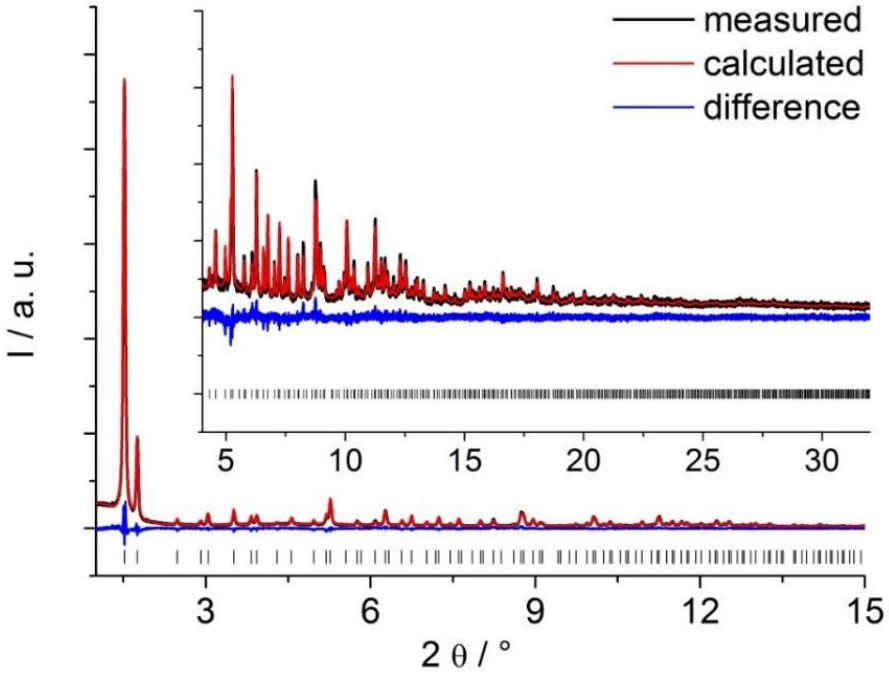

Figure S1 Final Rietveld plot for the refinement of Zr-UiO-66 (λ = 0.31783 Å). The black line shows the measured data, the red line shows the fit and the blue line is the difference curve. Vertical bars mark the allowed peak positions. The inset shows a magnification at higher angles.

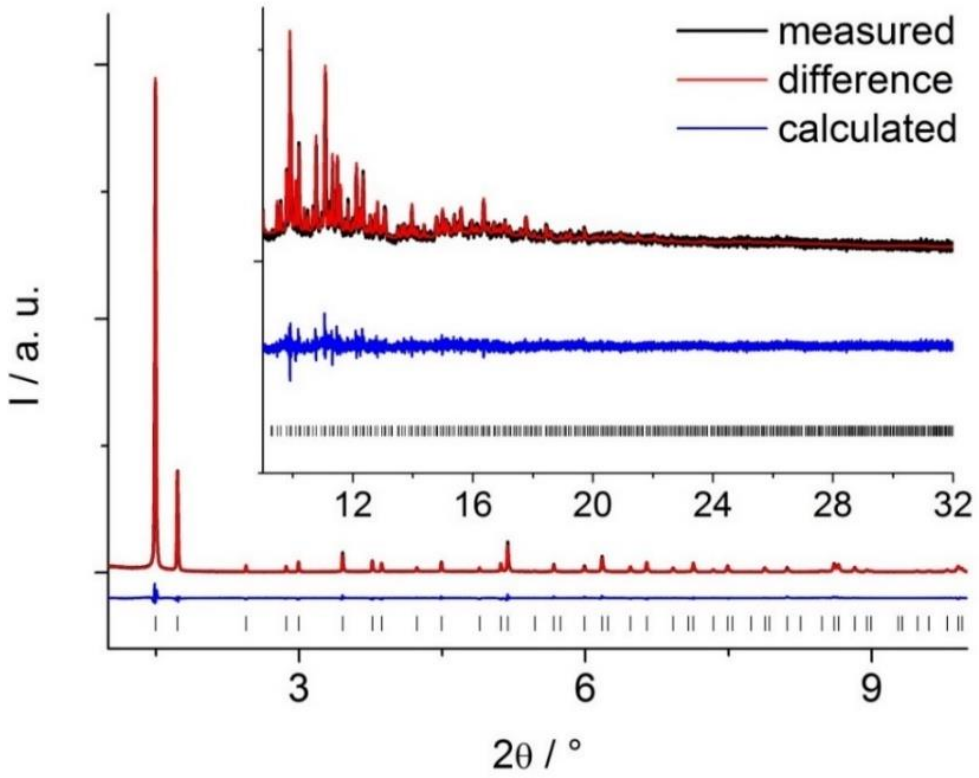

Figure S2 Final Rietveld plot for the refinement of $Zr_{3.54}Ce_{2.46}$-UiO-66 (λ = 0.31783 Å). The black line shows the measured data, the red line shows the fit and the blue line is the difference curve. Vertical bars mark the allowed peak positions. The inset shows a magnification at higher angles.

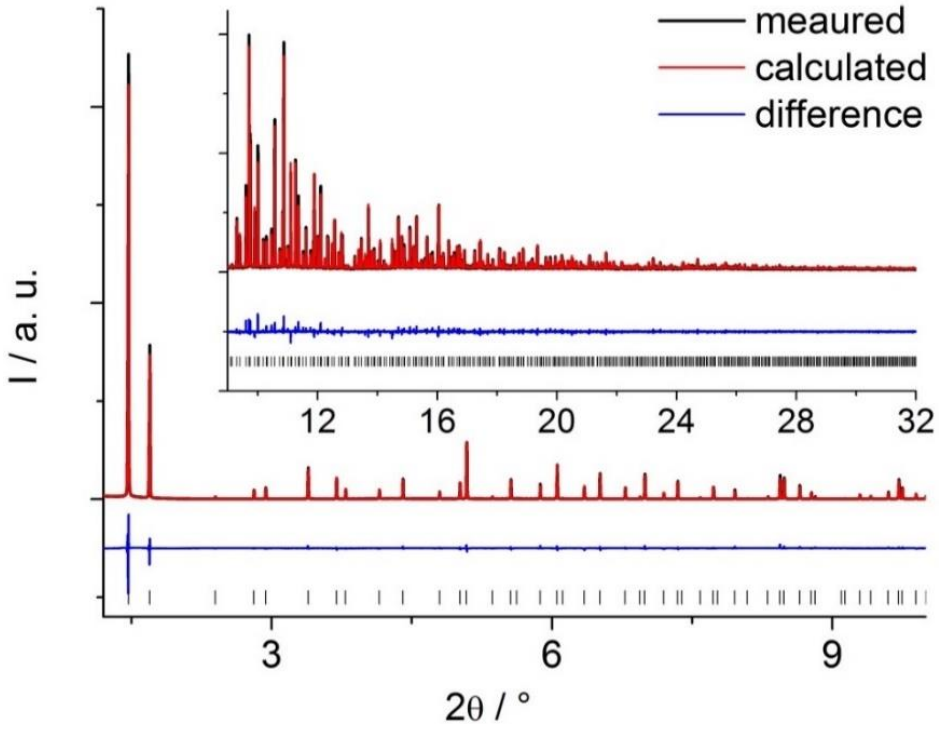

Figure S3 Final Rietveld plot for the refinement of Ce-UiO-66 (λ = 0.31783 Å). The black line shows the measured data, the red line shows the fit and the blue line is the difference curve. Vertical bars mark the allowed peak positions. The inset shows a magnification at higher angles.

Table S3 Results of PXRD refinement for pure Ce- and Zr- and mixed-metal Ce/Zr-UiO-66 MOFs

Compound	Zr-UiO-66	$Zr_{3.54}Ce_{2.46}$-UiO-66	Ce-UiO-66
Crystal system	cubic	cubic	cubic
Space group	*Fm*-3*m*	*Fm*-3*m*	*Fm*-3*m*
$a = b = c$ [Å]	20.7535(2)	21.0652(1)	21.48825(2)
$\alpha = \beta = \gamma$ [°]	90	90	90
V [$Å^3$]	8938.75(26)	9347.52(14)	9922.09(2)
Metal:linker ratio (ideally 6:6)	6 : 5.5	6 : 5.9	6 : 5.7
Distance restrains	5	5	5
R_{WP} [%]	7.3	8.7	8.5
R_P [%]	5.7	6.3	6.9
R_{Bragg} [%]	2.7	3.0	2.4
GoF	4.9	6.5	7.8
M-M distance [Å] (M= Ce, Zr)	3.51	3.67	3.78

4. XAS

4.1 Experimental

All XAS measurements except for those for Ce10 sample were performed at BM31 beamline[5] of European Synchrotron Radiation Facility (ESRF, Grenoble, France). The ring was operating in 7/8 multibunch mode with the current between 160 and 200 mA. All the measurements at BM31 were conducted in transmission mode using Si (111) double-crystal monochromator. Three ionization chambers were used for photon detection (30 cm long, 1 bar filing, 1 kV voltage). Gas mixtures used for filling the ionization chambers and resulting absorption values are given in Table S4.

Table S4 Filling the ionization chambers for the XAS experiments reported

Edge	Edge energy, eV	I_0 mixture and resulting absorption at the edge	$I_{1,2}$ mixture and resulting absorption at the edge
Ce L_3	5723	30% N_2 in He (18 %)	10% Ar in He (70%)
Zr K	17998	30% Ar in He (15 %)	10 % Kr in Ar (74%)
Ce K	40 443	15% Kr in Ar (15%)	100% Kr (57%)

XAS spectra for Ce10 sample were collected at BM23 beamline[6] of the ESRF. The experimental setup was similar to the one at BM31, except for the use of Si (311) monochromator for the measurements at Ce K-edge. The effect of higher resolution of Si (311) crystal compared to Si (111) was taken into account during the fitting of the EXAFS spectra of Ce10 sample, as described in the Section 4.4.

All MOFs were measured in the form of self-supporting pellets of 5 mm diameter, pressed using the pressure lower than 500 kgf/cm^2. The mass of MOF powder for sample preparation was optimized by XAFSmass software.[7]

4.2 XANES

Ce L_3 edge XANES data demonstrate, that Ce in all studied compounds is predominantly in Ce(IV) oxidation state (Figure S4a).

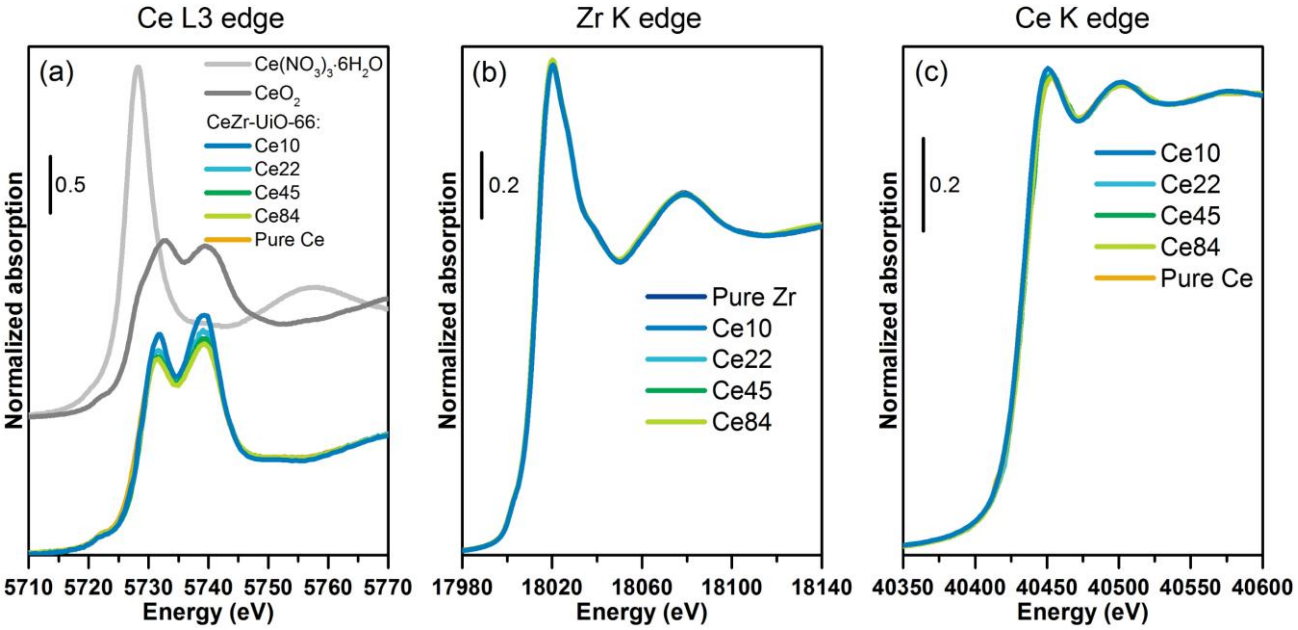

Figure S4 Ce L_3 (a), Zr K and Ce K-edge XANES spectra of bimetallic CeZr-UiO-66 MOFs compared to the spectra of pure Ce- and Zr-UiO-66 and (panel a) to the spectra of reference Ce (III) and Ce(IV) compounds

XANES spectra of pure and bimetallic MOFs are very similar at each of the three absorption edges, which confirms the similarity of local geometry and electronic structure of Zr and Ce centers in these MOFs at different Ce:Zr ratios, indicating that we are dealing with an isomorphous substitution of Ce in Zr sites and that no measurable extra phase is formed. This observation confirms the absence of the extra-phases, including the amorphous ones, generalizing thus the conclusion drawn using the XRD regarding the absence of crystalline extra-phases.

4.3 EXAFS data overview

XAFS data analysis was performed using Athena program for averaging and normalizing data and Artemis code for EXAFS fitting, both codes coming from Demeter package.[8] The data quality was good, which allowed the EXAFS data collection up to k=20 Å^{-1} at Ce and Zr K-edges for most samples, but in order to compare the data of different samples in the same range, the Fourier transform were performed in the 3.65-16.8 Å^{-1} (Zr K-edge) and 4-16.8 Å^{-1} range (Ce K-edge), limited by signal-to-noise ratio for the samples with the lowest concentration of Ce and Zr (Figure S5).

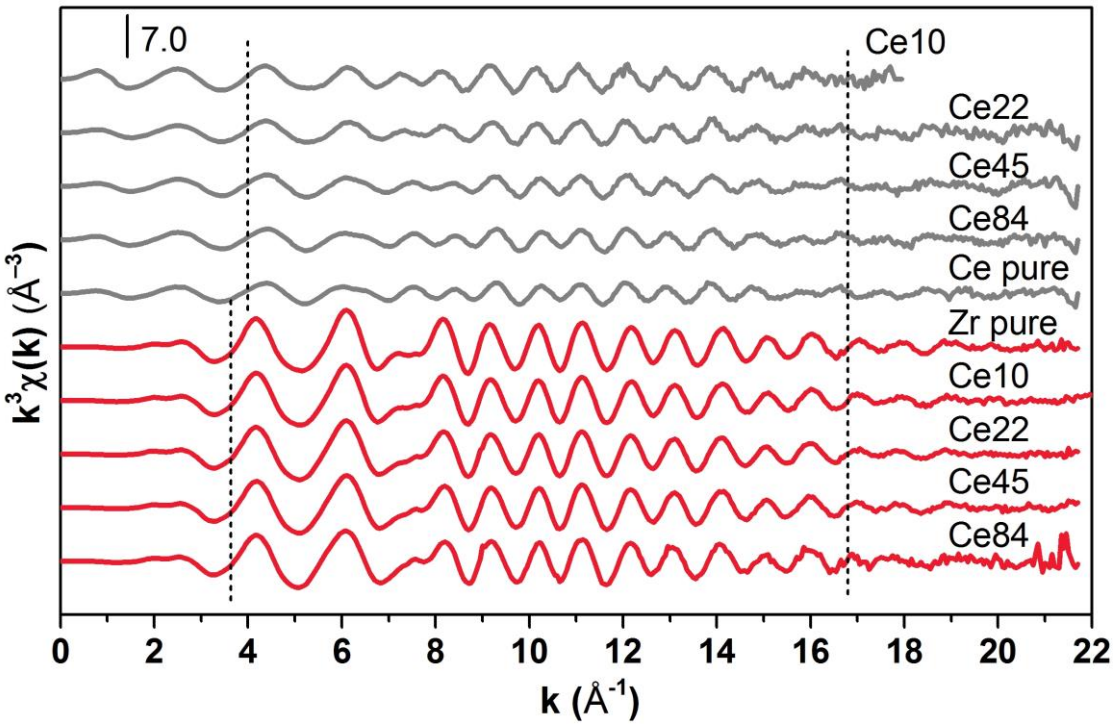

Figure S5 $k^3\chi(k)$ EXAFS data at Ce (gray) and Zr K-edges (red) for pure and bimetallic Ce/Zr-UiO-66 materials. Dashed lines indicate the regions used for the Fourier transform.

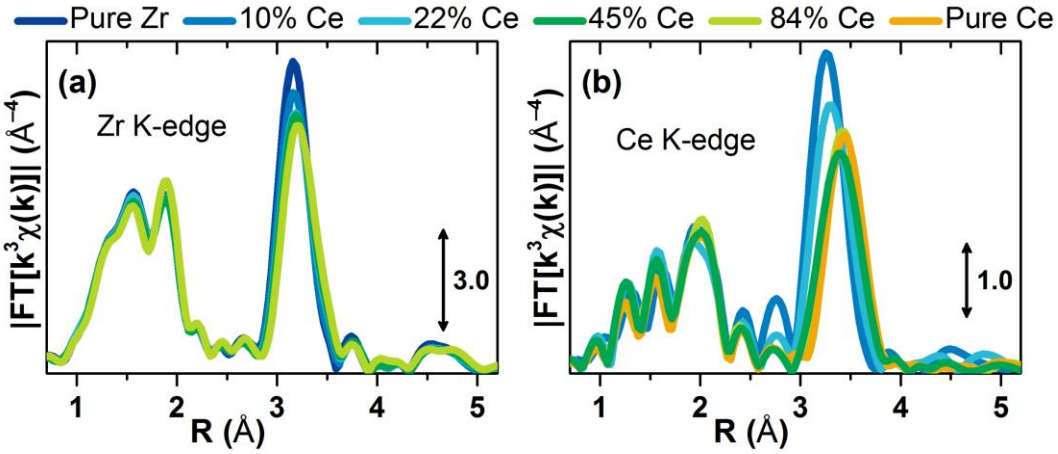

Figure S6 Moduli of the phase-uncorrected Fourier transforms of k^3-weighted EXAFS data collected at (a) Zr K-edge and (b) Ce K-edge for UiO-66 MOFs with pure Zr-, pure Ce-, and mixed Ce/Zr cornerstones.

k^3-weighted, Fourier-transformed Zr and Ce K-edge EXAFS data for all MOFs are shown in the Figure S6. Notably, the evolution of the second EXAFS peak is quite different between Zr and Ce K-edges. Indeed, for the case of Zr K-edge, its intensity is at maximum for the pure material. Upon introduction of 22% of Ce the peak decreases significantly and shifts to higher R. However, further increase of Ce fraction in the material has very little effect on both intensity and position of the maximum. Conversely, at the Ce K-edge the Ce–M peak is most intense for the Ce10 sample. Its intensity reaches a minimum for the Ce45 sample, and then stabilizes at an intermediate value for

the MOFs with the highest Ce-content. Gradual shift of the peak to the higher R values indicates that the increase of Ce content in the material leads to an elongation of the average Ce–M distance.

4.4 EXAFS fit parametrization

Structure and composition of cornerstones being the target, the fit was performed in R-space in the region where the signal from M–M scattering is dominant. Therefore, spectra of mixed-metal MOFs were fitted taking only M–M scattering paths into account. Initial values for interatomic Zr–Zr and Ce–Ce distances were taken from the refined PXRD data of the pure Zr and Ce MOFs respectively. For Zr–Ce and Ce–Zr paths the same initial distance as for Zr–Zr path was adopted. Based on the qualitative considerations discussed in the main text, degeneracies of the paths were calculated assuming that in the Ce22, Ce45 and Ce84 materials only $CeZr_5$ and Ce_6 clusters are present, while Ce10 MOF is built with $CeZr_5$ and Zr_6 ones. In all cases the total coordination number of the absorbing atom (Zr or Ce) was set to 4. Assuming such composition of the MOFs and using the total Ce/Zr ratio provided by EDX for each material, corresponding degeneracies of different M-M scattering paths, fraction of pure cornerstones as well as other parameters were calculated and presented in the Table S5. Notably, substantial deviation of the relative degeneracies of Ce–Ce and Ce–Zr paths from the molar Ce:Zr ratio can be observed for high-Ce materials. This is the case because each Ce_6 cornerstone contributes to the EXAFS data by 24 Ce–Ce scattering paths, in contrast to only four Ce-Zr paths from every $CeZr_5$ cluster, which leads to a very fast rise of the Ce-Ce contribution to the Ce K-edge EXAFS with the increase of Ce content. Degeneracies of the Ce–Ce and Ce–Zr paths, reported in Table S5 and calculated from purely stoichiometric considerations, were fixed during the EXAFS fitting, being the characteristic fingerprint of the adopted model.

Table S5 Stoichiometric parameters for mixed-metal MOFs calculated under assumption of preferential formation of $CeZr_5$ cornerstones.

Sample	Ce content, %	Zr content, %	Fraction of pure cornerstones*	Fraction of $CeZr_5$ cornerstones	Ratio Ce-Ce/Ce-Zr paths	Degeneracy Ce-Ce path, Ce K-edge	Degeneracy Ce-Zr path, Ce K-edge	Degeneracy Zr-Zr path, Zr K-edge	Degeneracy Zr-Ce path, Zr K-edge
Ce10	10	90	0.4	0.6	0	0	4	3.56**	0.44
Ce22	22	78	0.064	0.936	0.41	1.16	2.84	3.2	0.8
Ce45	45	55	0.34	0.66	3.09	3.02	0.98	3.2	0.8
Ce84	84	16	0.808	0.192	25.25	3.85	0.15	3.2	0.8

* Pure cornerstones are Zr_6 for Ce10 and Ce_6 for Ce22, Ce45 and Ce84

** For Ce10 the Zr-Zr path was split into two, corresponding to Zr-Zr scattering in Zr_6 and $CeZr_5$ cornerstones. Degeneracy of each of these two sub-paths was set to 1.78 in the fit, proportional to the number of the Zr-Zr paths in the corresponding cornerstone weighted by abundance of the latter.

In order to decrease the number of parameters and increase the stability of the fit, the spectra of the Ce and Zr K-edges for pure Zr- and Ce-UiO-66 and mixed-metal Zr/Ce-UiO-66 MOFs were fitted together, sharing most of the fitting parameters. In particular, common amplitude reduction factor S_0^2 was used for all the spectra, which is justified by the structural similarity of the studied compounds and confirmed by previously reported data for Zr and Ce K-edges of similar systems.[9-

[10] Then, since XANES spectra at the same edge are very similar for all compounds (Figure S4), only two energy shift parameters were used for the fitting: ΔE_{Ce} and ΔE_{zr} for Ce and Zr K-edge, respectively. To maintain consistency of the results, the same interatomic distance and Debye Waller (DW) factor were assigned to the Zr–Ce paths at Zr K-edge and Ce–Zr paths at Ce K-edge. Analogously, the Ce-Ce distance and corresponding DW factor were constrained to be equal for Ce–Ce paths in mixed-metal and pure Ce MOFs, since within the adopted model these paths originate in both cases from pure Ce_6 cornerstones. This choice is also justified by the fact that when independent parameters for Ce–Ce distance and DW factor for the pure Ce MOF were introduced in the fit, the obtained values were within the errors from analogous parameters for mixed-metal compounds. Conversely, independent Zr–Zr distance and DW parameters were assigned to the Zr–Zr paths in the Zr_6 and $CeZr_5$ cornerstones. Notably, Zr-Zr contribution in the Ce10 sample was fitted with two different Zr-Zr scattering paths, since both Zr_6 and $CeZr_5$ clusters were expected to be present in the sample.

Since Ce K-edge data for Ce10 sample were measured with Si(311) monochromator in contrast to the Si(111) used for all other samples, a correction to the DW factor for Ce-Zr scattering path of Ce10 was introduced, to account for the higher resolution of the Si(311) crystal and therefore more intense peaks in the EXAFS FT. To estimate the value for the necessary correction, the EXAFS spectrum of pure Ce-UiO-66 was measured using both Si(111) and Si(311) crystals and fitted fixing the S_0^2 and ΔE_{Ce} parameters to the values obtained during the combined fitting of all the spectra except for those of Ce10. Obtained results are presented in the Figure S7.

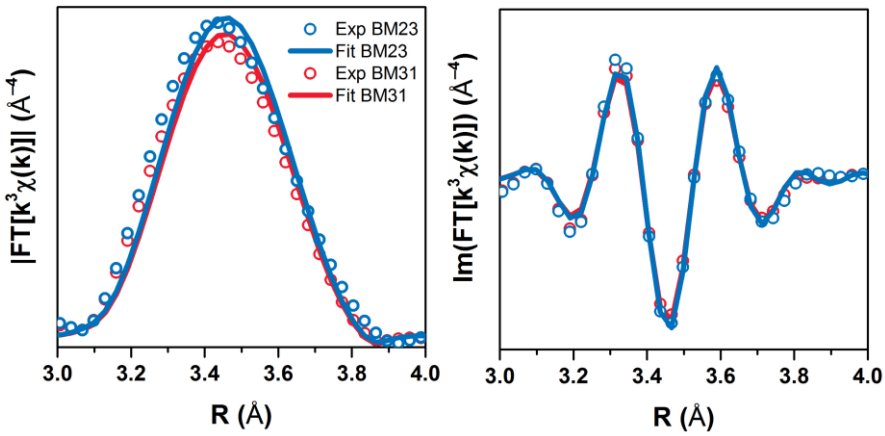

Figure S7 Results of the fitting of the EXAFS spectrum of pure Ce-UiO-66 MOF collected at BM31 and BM23 beamlines with Si (111) and Si (311) monochromators respectively.

While the difference in the obtained Ce-Ce distances was, as expected, negligible, the resulting difference in the DW factors for the two datasets was 0.0002 $Å^2$. This value was therefore used to correct the DW factor for the Ce10 MOF during the global refinement, introducing the relation (S1)

$$\sigma^2_{Ce\text{-}Zr}(Ce10) = \sigma^2_{Ce\text{-}Zr}(global) - 0.0002\ (Å^2) \qquad (S1)$$

4.5 EXAFS fitting results

Under constraints described in the previous section all the parameters were freely varied during the simultaneous fit of all the ten datasets, resulting in the calculation of the global R-factor.

Fit results for all compounds are shown in Figure S8, Figure S9, Figure S10, Figure S11, and Figure S12

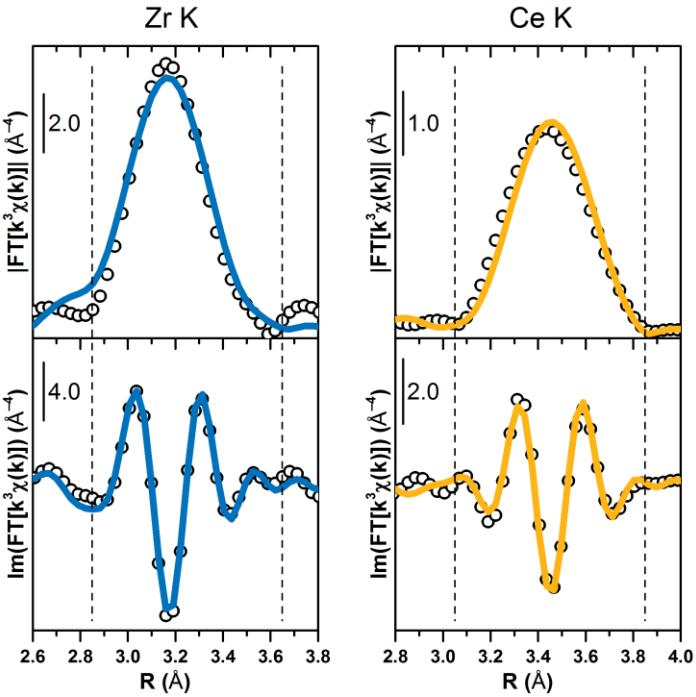

Figure S8 Results of the EXAFS fitting for pure Zr- and Ce-UiO-66 MOFs: experiment (circles) and fit (solid lines).

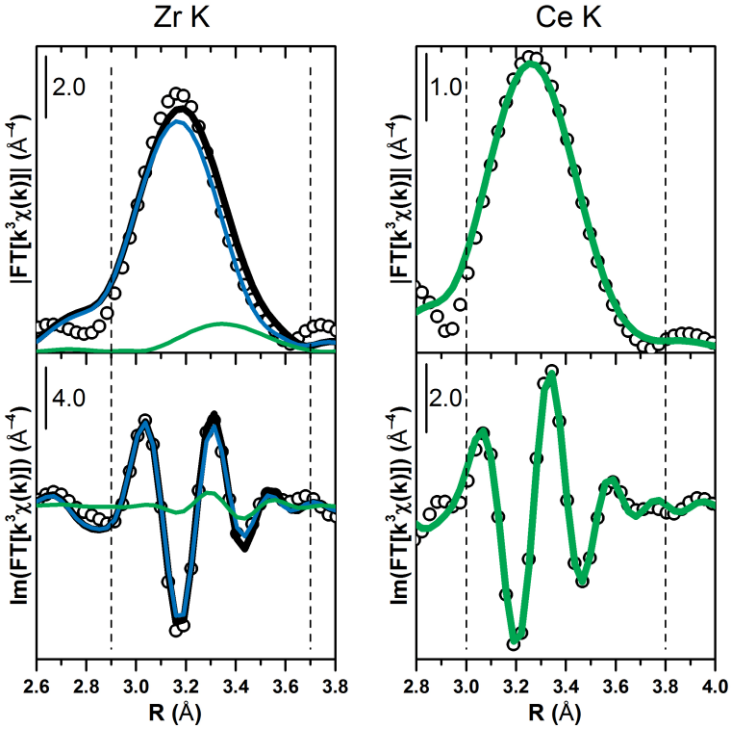

Figure S9 Results of the EXAFS fitting for Ce10 MOF: experiment (circles) and fit (black solid lines). Contribution to the fit from Zr-Zr and Zr-Ce (Ce-Zr) scattering is shown by blue and green lines respectively.

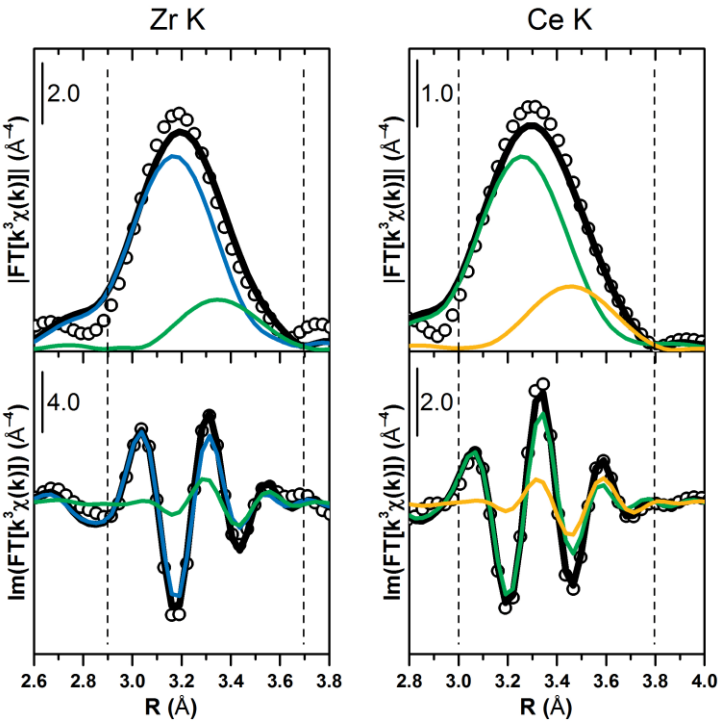

Figure S10 Results of the EXAFS fitting for Ce22 MOF: experiment (circles) and fit (black solid lines). Contribution to the fit from Zr-Zr, Ce-Ce and Zr-Ce (Ce-Zr) scattering is shown by blue, yellow and green lines respectively.

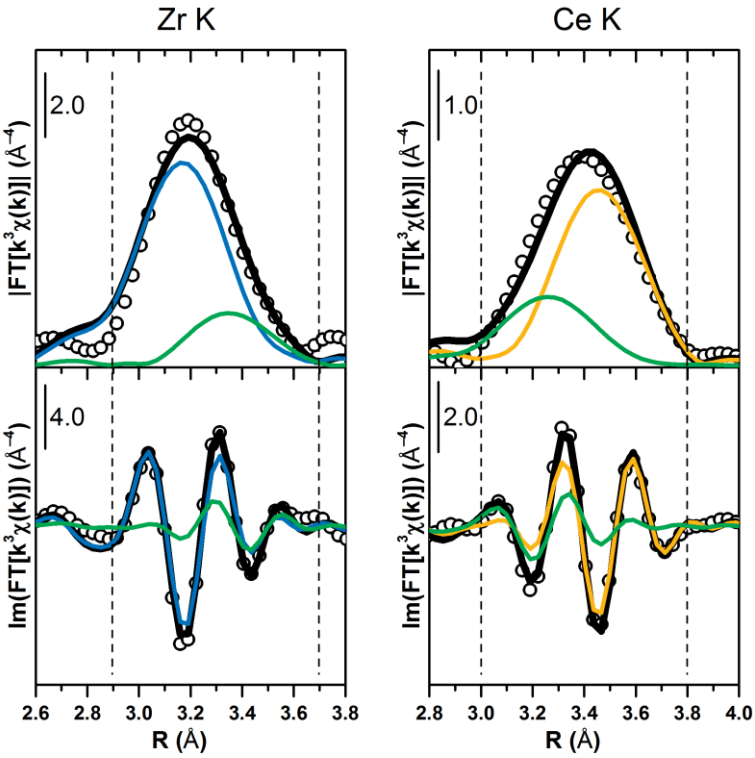

Figure S11 Results of the EXAFS fitting for Ce45 MOF: experiment (circles) and fit (black solid lines). Contribution to the fit from Zr-Zr, Ce-Ce and Zr-Ce (Ce-Zr) scattering is shown by blue, yellow and green lines respectively.

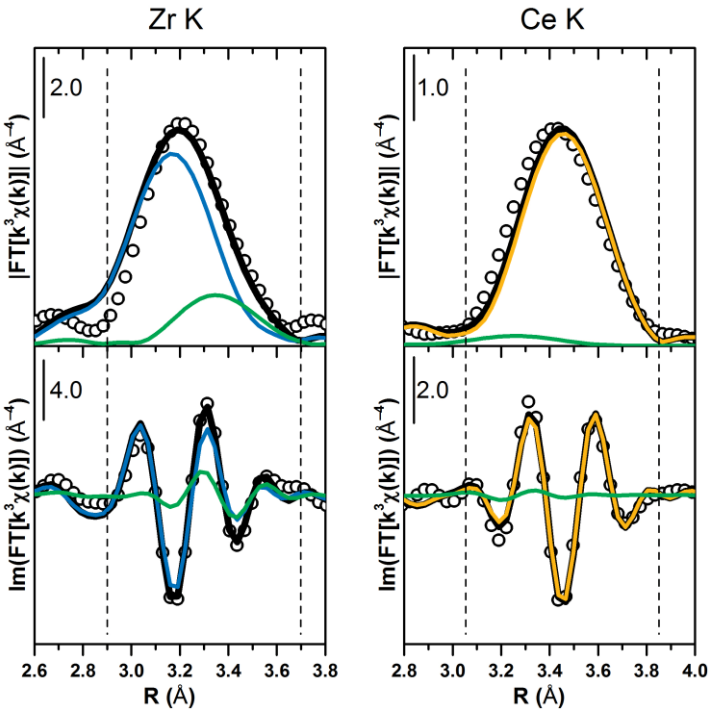

Figure S12 Results of the EXAFS fitting for Ce84 MOF: experiment (circles) and fit (black solid lines). Contribution to the fit from Zr-Zr, Ce-Ce and Zr-Ce (Ce-Zr) scattering is shown by blue, yellow and green lines respectively.

In order to assess the quality of each individual fit, the corresponding R-factors were calculated and presented in the Figure S13. For all the datasets the R-factors are quite low, the highest being 0.021 for the Zr K-edge of Ce84 MOF.

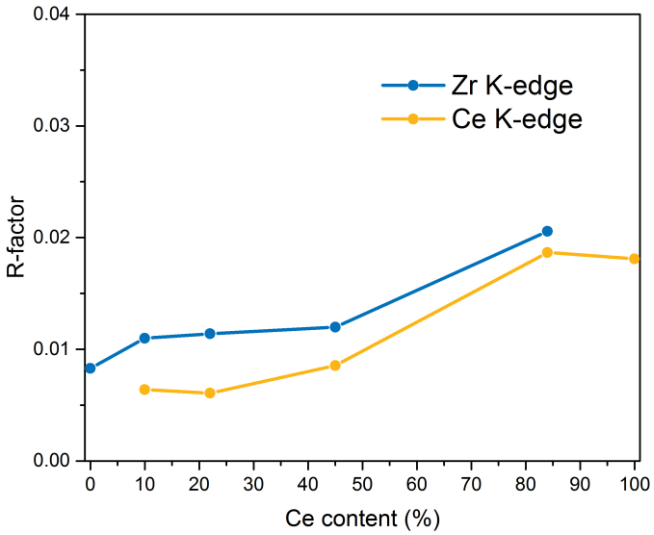

Figure S13 Individual R-factors obtained during the combined refinement of the ten datasets of pure and bimetallic Ce/Zr-UiO-66 MOFs.

5. DFT calculations

Stability of the M_6 cornerstone of UiO-66 MOF with different Ce/Zr ratio was assessed by means of DFT calculations performed in VASP 5.3 code.[11-13] The local environment of the cluster was truncated after the nearest carbons of the linkers, which were terminated by hydrogens to

compensate for the unsaturated bonds. For each symmetry non-equivalent model of the bimetallic cluster geometry optimization was performed and the total energy was calculated. PBE exchange-correlation potential was used. The energy cutoff value of 400 eV was taken for the plane-wave basis set. All calculations were performed with one single k-point.

The energy cost of allocating one Ce atom as a part of a mixed cornerstone was calculated using the formula:

$$\Delta E_{\mathrm{Ce}} = \frac{E - E_0}{N_{\mathrm{Ce}}}$$

where E is the energy of the specific cluster, E_0 is the energy of pure Zr cluster and N_{Ce} is the number of Ce atoms in the specific cluster. The choice of such figure of merit was justified by the fact that the amount of Ce in the real MOF is always fixed by the synthesis stoichiometry, and the goal is to find the most energetically favorable way to distribute these Ce atoms among the cornerstones.

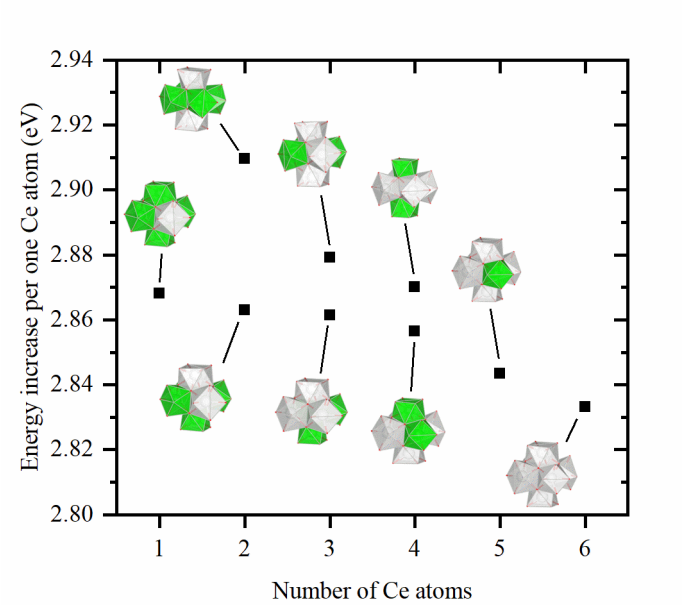

Figure S14 Allocation energies of one Ce atom in different cornerstones compared to the pure Zr_6 cluster

The results are reported in the Figure S14. In agreement with the findings of Trousselet et al,[14] the energies of formation of the bimetallic clusters are positive, making this process energetically unfavorable (at T = 0 K and P = 0 Pa). The calculations show, that the most energy-efficient way to allocate the given amount of Ce atoms is the formation of Ce_6 cornerstones, that have the lowest energy increase per Ce atom.

Thus, within this computational model, only the Zr_6 and Ce_6 clusters should be expected in the mixed metal UiO-66 MOFs. However, that would lead to the absence of changes in the Ce and Zr K-edge EXAFS spectra of the MOFs with different Ce content. Since it is not the case in the experiment, more complex computational models might be required to properly describe the phenomena that drive the formation of bimetallic MOFs.

References

(1) Lammert, M.; Wharmby, M. T.; Smolders, S.; Bueken, B.; Lieb, A.; Lomachenko, K. A.; Vos, D. D.; Stock, N. Cerium-based metal organic frameworks with UiO-66 architecture: synthesis, properties and redox catalytic activity. *Chem. Commun.* **2015**, *51*, 12578.

(2) Lammert, M.; Glißmann, C.; Stock, N. Tuning the stability of bimetallic Ce(IV)/Zr(IV)-based MOFs with UiO-66 and MOF-808 structures. *Dalton Trans.* **2017**, *46*, 2425.

(3) Cavka, J. H.; Jakobsen, S.; Olsbye, U.; Guillou, N.; Lamberti, C.; Bordiga, S.; Lillerud, K. P. A New Zirconium Inorganic Building Brick Forming Metal Organic Frameworks with Exceptional Stability. *J. Am. Chem. Soc.* **2008**, *130*, 13850.

(4) Coelho, A. *Topas Academics 4.2*, Coelho Software: Brisbane, Australia, 2007.

(5) Abdala, P. M.; Safonova, O. V.; Wiker, G.; van Beek, W.; Emerich, H.; van Bokhoven, J. A.; Sá, J.; Szlachetko, J.; Nachtegaal, M. Scientific Opportunities for Heterogeneous Catalysis Research at the SuperXAS and SNBL Beam Lines. *CHIMIA* **2012**, *66*, 699.

(6) Mathon, O.; Beteva, A.; Borrel, J.; Bugnazet, D.; Gatla, S.; Hino, R.; Kantor, I.; Mairs, T.; Munoz, M.; Pasternak, S.; Perrin, F.; Pascarelli, S. The time-resolved and extreme conditions XAS (TEXAS) facility at the European Synchrotron Radiation Facility: the general-purpose EXAFS bending-magnet beamline BM23. *J. Synchrotron Rad.* **2015**, *22*, 1548.

(7) Klementiev, K.; Chernikov, R. XAFSmass: a program for calculating the optimal mass of XAFS samples. *J. Phys.: Conf. Ser.* **2016**, *712*, 012008.

(8) Ravel, B.; Newville, M. ATHENA, ARTEMIS, HEPHAESTUS: data analysis for X-ray absorption spectroscopy using IFEFFIT. *J. Synchrotron Rad.* **2005**, *12*, 537.

(9) Smolders, S.; Lomachenko, K. A.; Bueken, B.; Struyf, A.; Bugaev, A. L.; Atzori, C.; Stock, N.; Lamberti, C.; Roeffaers, M. B. J.; De Vos, D. E. Unravelling the Redox-catalytic Behavior of Ce^{4+} Metal-Organic Frameworks by X-ray Absorption Spectroscopy. *ChemPhysChem* **2018**, *19*, 373.

(10) Waitschat, S.; Fröhlich, D.; Reinsch, H.; Terraschke, H.; Lomachenko, K. A.; Lamberti, C.; Kummer, H.; Helling, T.; Baumgartner, M.; Henninger, S.; Stock, N. Synthesis of M-UiO-66 (M = Zr, Ce or Hf) employing 2,5-pyridinedicarboxylic acid as a linker: defect chemistry, framework hydrophilisation and sorption properties. *Dalton Trans.* **2018**, *47*, 1062.

(11) Kresse, G.; Furthmüller, J. Efficiency of ab-initio total energy calculations for metals and semiconductors using a plane-wave basis set. *Comput. Mater. Sci.* **1996**, *6*, 15.

(12) Kresse, G.; Furthmüller Efficient iterative schemes for ab initio total-energy calculations using a plane-wave basis set. J., *Phys. Rev. B* **1996**, *54*, 11169.

(13) Kresse, G.; Joubert, D. From ultrasoft pseudopotentials to the projector augmented-wave method. *Phys. Rev. B* **1999**, *59*, 1758.

(14) Trousselet, F.; Archereau, A.; Boutin, A.; Coudert, F.-X. Heterometallic Metal–Organic Frameworks of MOF-5 and UiO-66 Families: Insight from Computational Chemistry. *J. Phys. Chem. C* **2016**, *120*, 24885.